Compositional dependence of the elastic constants and the lattice parameter of $Al_xGa_{1-x}As$

S. Gehrsitz and H. Sigg
Paul Scherrer Institut, Labor für Mikro- and Nanostrukturen, Badenerstrasse 569, CH-8048 Zürich, Switzerland

N. Herres, K. Bachem, and K. Köhler
Fraunhofer Institut für Angewandte Festkörperforschung, Tullastrasse 72, D-79108 Freiburg im Breisgau, Germany

F. K. Reinhart
Institute de Micro- et Optoelectronique, EPFL, CH-1015 Lausanne, Switzerland
(Received 1 March 1999)

Near infrared Brillouin scattering and high resolution x-ray diffraction is used for a precise determination of the elastic constants and the relaxed lattice parameters of $Al_xGa_{1-x}As$ epitaxial layers ($0.1 \leqslant x \leqslant 1.0$). The composition of the layers is specified by inductively coupled plasma atomic emission spectroscopy, photoluminescence, and Raman spectroscopy. For the elastic constants we get a composition independent value of 118.9 ± 0.7 GPa for C_{11}, a nonlinear increase in C_{12} and a linear decrease in C_{44} with increasing Al composition. The Poisson ratio shows a linear increase for $x < 0.8$ and a downward bowing for higher Al concentrations to the AlAs value of $\nu = 0.325 \pm 0.004$. The effect of lattice mismatch induced strain on the elastic properties is investigated on free standing epitaxial layers. The trend in ionicity from the GaAs to the AlAs bonds are deduced from phenomenological expressions for the bond-bending and bond-stretching forces which are calculated from the elastic constants. The lattice parameters of the unstrained crystals are obtained from the measured full metric of the tetragonally strained layers and the Poisson ratios. The combined results of Brillouin scattering, x-ray diffraction, and compositional analysis confirm the deviation of the $Al_xGa_{1-x}As$ lattice parameter from Vegard's law, and provides the first direct and accurate determination of the quadratic bowing parameter. [S0163-1829(99)14439-4]

I. INTRODUCTION

Among the various techniques for the determination of the Al composition of ternary III-V and II-VI epitaxial layers, high resolution x-ray diffraction (HRXRD) is the most popular one due to its high accuracy and nondestructive character. In the case of the technolocigally important $Al_xGa_{1-x}As/GaAs$ system, however, there has been a controversial debate in recent years on the assumptions underlying the evaluation of the x-ray data.[1] In nearly all HRXRD studies on $Al_xGa_{1-x}As$ epitaxial layers published recently[2–8] the most fundamental assumption is the rigid commitment to Vegard's law,[9] that postulates a linear relationship between the relaxed lattice constant and the composition x. To get the composition of a pseudomorphically grown epitaxial layer from the measured strained lattice mismatch, the lattice parameter and the Poisson ratio of the binary compounds ($x = 0$ and $x = 1$) have to be known very precisely. One reason for the large scatter in the published relations between the observed HRXRD peak-splitting and the Al-content x is the lack of reliable data on the elastic constants of $Al_xGa_{1-x}As$. Usually it is assumed that the Poisson ratio of the mixed crystal varies linearly with composition, but an accurate HRXRD composition determination demands the knowledge of its composition dependence. The question of the applicability of Vegard's law for the interpretation of x-ray rocking curves is crucial. In recent years some hints were given that Vegard's law does not hold in the $Al_xGa_{1-x}As$ system.[10,11]

This motivated us to remeasure our recently published elastic constants[13] with higher accuracy, and to determine the composition of our samples independently by various techniques, such as photoluminescence (PL), Raman spectroscopy, and inductively coupled plasma atomic emission spectroscopy (ICP-AES). The combination of the compositional data with the results from the Brillouin and HRXRD measurements provide the accurate dependence of the relaxed lattice parameter as a function of composition. Unlike in other studies,[11] we determine the lattice parameter and the composition directly from data obtained by independent measurements on the same samples without any additional assumptions or fitting procedures.

II. EXPERIMENTS

A. Compositional analysis

The $Al_xGa_{1-x}As$ layers are grown by MBE and MOCVD on semi-insulating (001) GaAs substrates. The layers are embedded between thin GaAs buffer and cap layers. SIMS measurements reveal a carbon incorporation for the MOCVD samples of less than 2×10^{17} cm^{-3}. The free carrier concentration of some samples is determined by Hall measurements and yielded values below 10^{17} cm^{-3}. The sample parameters can be found in Table I. The composition has been determined using the following independent techniques.

1. Optical measurements (PL and Raman spectroscopy)

Photoluminescence experiments are performed using a 0.64-m Czerny-Turner grating monochromator with slit widths of $50-100$ μm at temperatures of $2-4$ K. The

 ©1999 The American Physical Society

TABLE I. Sample parameter.

Sample	Growth	Aluminum fraction (x) Optic[a]	ICP-AES	HRXRD[b]	Thickness (μm)
P	MOCVD	0.095 ± 0.005		0.112 ± 0.008	1.0
B	MOCVD	0.170 ± 0.005	0.176 ± 0.005	0.192 ± 0.005	5.0
F	MBE	0.225 ± 0.005		0.247 ± 0.005	2.0
C	MOCVD	0.325 ± 0.005	0.334 ± 0.005	0.369 ± 0.005	10.4
A	MOCVD	0.405 ± 0.015	0.410 ± 0.005	0.437 ± 0.006	4.8
D	MOCVD	0.619 ± 0.015	0.615 ± 0.005	0.646 ± 0.007	9.0
N	MOCVD		0.753 ± 0.005	0.779 ± 0.008	5.0
Q	MOCVD		0.865 ± 0.005	0.869 ± 0.01	4.9
E	MOCVD	AlAs	0.998 ± 0.005	AlAs	7.8

[a]According to the calibration curves of Wasilewski *et al.* (Ref. 11).
[b]Assuming Vegard's law.

samples are excited with an Ar^+-ion laser operating at $\lambda = 488$ nm with excitation power densities ranging from 1 mW/cm^2 to 2 W/cm^2. To unambiguously identify the energy of the donor-bound exciton (D^0,X), which is usually used for composition determination, we additionally performed photoluminescence excitation by using a white light lamp in combination with a second grating spectrometer. For the direct-gap samples (P, B, C and F) we determined the Al-content from the (D^0,X) energies using the calibration curve proposed by Wasilewski *et al.*[11]

For indirect-gap $Al_xGa_{1-x}As$ ($x > 0.38$) the interpretation of PL spectra is ambiguous and yield a reduced compositional resolution.[11] We therefore use Raman spectroscopy to determine the Al-content for the samples with $x > 0.4$. The Raman scattering experiments are performed at room temperature for near backscattering condition from the (001) growth surface. The samples are excited with 100 mW of the 514.5 nm line of the Ar^+-ion laser with a spot size of 50 μm diam at the sample surface. The scattered light is dispersed by a double grating spectrometer with a spectral resolution of 3 cm^{-1}. From the energies of the GaAs-like and the AlAs-like LO phonons, we determine the Al-content by using the compositional dependence of these peaks as given in Ref. 11.

2. ICP-AES Analysis

Although ICP-AES is very well known for compositional analysis in semiconductor processing[14] it has never been used, as far as we know, as a characterization tool for the composition of ternary epitaxial layers. The technique is based on the spectroscopic identification of the characteristic atomic emission of the constituents. Basically, the epitaxial layer has to be dissolved by an acid solution (1:1 mixture of HNO_3/HCl) and then it is carried by argon gas to a plasma torch. The solutes are evaporated by an inductively coupled plasma and excited to high temperatures (up to 10^4 K) available in the argon plasma. When the excited atoms relax to their ground state, the specific emission of the species can be detected. Usually this technique is used as an analytical tool for trace metal analysis. When using the method for the composition determination of semiconductor alloys, it provides very accurate results. Only a relative measurement of the characteristic emission intensities of the elements is necessary. With properly calibrated standard solvents, the specified[15] measurement uncertainty is below 0.3 at. %. However, prior to the ICP-AES analysis a careful sample preparation is required. For an accurate composition determination the GaAs substrate and cap layer have to be removed completely by chemical etching. For samples with $x > 0.3$ we use the citric acid/hydrogen peroxide etch,[16] while for $x < 0.3$ the ammonium hydroxide/hydrogen peroxide etch[17,18] is used. The limited etch selectivity between GaAs and $Al_xGa_{1-x}As$, especially for low x, may cause a systematic error to lower Al-contents of the order of 0.001. To test the capabilities of the method, we investigate two specimen of the same wafer with a 9 μm thick $Al_{0.61}Ga_{0.39}As$ layer. On both specimen the substrate is removed, but the thin (≈ 10 nm) GaAs cap layer was etched off only on one sample. For the layer with the GaAs cap, we obtain a composition value 0.15 at. % lower than for the sample without cap. From this result we conclude that ICP-AES is capable of resolving compositional differences of the order of 0.2 at. %. This is also consistent with the result obtained for the pure AlAs layer, where an AlAs/GaAs composition ratio of 0.998 is measured (Table I). We thus conclude that the absolute composition accuracy, including all systematic and statistical errors, in all cases is better than $\Delta x = \pm 0.005$.

The results of the compositional analysis are summarized in Table I. The values of the various techniques agree well with each other within the given uncertainties. Since the optical data rely on the calibration curves of Ref. 11, we conclude that the *in situ* composition calibration during MBE growth described by Wasilewski *et al.* provides accurate results, comparable to the *ex situ* chemical analysis by ICP-AES.

B. HRXRD measurements

A diffractometer as schematically shown in Fig. 1 is used for the HRXRD measurements. It is equipped with a Bartels-DuMond–type[19] germanium monochromator, a four-circle Eulerian cradle for sample and detector positioning and a high resolution optical encoder to accurately measure the angular position, with a resolution of 0.0001° and an absolute accuracy of 0.0003°. The wavelength of the Cu $K\alpha_1$ radiation ($\Lambda \approx 0.15406$ nm) is calibrated with a zone-refined silicon {111} crystal. If accurate angle reading

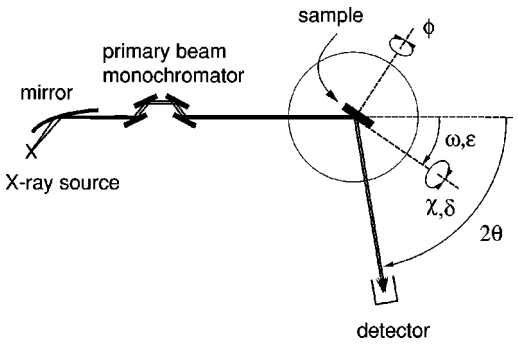

FIG. 1. Schematical view of the high resolution x-ray diffraction set-up.

(<1 arcsec) is ensured, the total error for the wavelength can be as low as 1 ppm. The samples are aligned on a two-arc goniometer head inside the Eulerian cradle with the normal of the growth surface ([001] crystal direction) parallel to the ϕ axis to better than 0.01° (Fig. 1). Additionally, a zone axis ([100] or [110]) is aligned parallel to the ω axis with an accuracy of 0.03° by using GaAs 444 asymmetric reflections. By employing a modified Bond technique,[20,21] all accessible reflections in this zone can then be measured at $+2\Theta$ and -2Θ detector settings without movement on any axis except ω and 2Θ. After completing the measurements in one zone the next zone axis is automatically set parallel to ω via a ϕ rotation. To enhance the accuracy, the ω position is measured at each step independently and is interpolated after completion of each reflection range. To measure the lattice parameters of the tetragonally strained layer and substrate the symmetrical (004, 006) and asymmetrical (115, 224, 206, 335, 444) reflections (measured in grazing incidence and grazing exit) are scanned subsequently. For evaluation, Gaussian profiles are fitted to the observed reflections and corrections are made for temperature and refraction. All results on the lattice parameters are given for $T=22.5$ °C.

The measurement technique we use in this study ensures that the common problems associated with thick (>1 μm) films, such as partial relaxation of the layer and deformation of the substrate, are properly taken into account. The effect of partial relaxation can lead to systematic errors in x-ray studies where only symmetrical reflections are used since only the lattice mismatch perpendicular to the growth surface is measured. Here we use symmetrical and asymmetrical reflections to determine the lattice constants for both, the layer and the substrate perpendicular and parallel to the surface independently from each other. Defect induced partial relaxation of the film with respect to the substrate, evidenced by different in-plane lattice constants of the layer and the substrate, does not pose a problem for the calculation of the unstrained lattice parameter, as long as the layer is tetragonally strained on the average.

It is also important to note at this point that our technique makes no use of the substrate lattice parameters in order to determine the layer lattice constants, in contrast to conventional x-ray rocking curves where only the peak separation between the substrate and the layer is measured. In particular, the results on the layer lattice constants are not influenced by a wafer curvature (resulting from thermal mismatch) leading to an inhomogeneous strain field in the layer, since the inhomogeneous contribution is small compared to the total strain of the film. Nevertheless, to avoid problems associated with sample curvature, we took care to position the sample surface in the center of the Eulerian cradle in such a way that the irradiated spot on the sample was only insignificantly displaced when moving from one *hkl* reflection to the next. Problems related to reflection dependent sampling depths do not affect the measurements of the layer lattice constants, because the penetration depths of the reflections used here are sufficiently large to average over the thickness of the layer.

The substrate however is inhomogeneously strained along the growth direction with a tensile strain near the growth surface and a compressive strain at the backside. Thus for the determination of the lattice parameters of a substrate covered with a thick layer, different sampling depths of the various x-ray reflections (hkl) have to be taken into consideration.[22] In conventional x-ray studies this effect is often neglected or it is even assumed that the substrate is completely unstrained.

To conclude, we point out that the lattice constants of the strained layers are determined here without recurrence to the substrate as an internal standard and are solely based on the $Al_xGa_{1-x}As$ peak position and the calibrated x-ray wavelength.

C. Brillouin measurements

Near infrared Brillouin scattering has become a versatile technique for the investigation of elastic properties of transparent III-V epitaxial layers.[13,23] By using excitation energies below the bandgap of the material, the usual opacity broadening of the Brillouin lines of opaque semiconductors[24] is avoided. This permits the precise determination of the Brillouin shifts from bulk acoustic phonons. The elastic constants of the sample can then be deduced with high accuracy. Earlier results of near infrared Brillouin scattering on $Al_xGa_{1-x}As$ epitaxial layers can be found in Refs. 12 and 13. These measurements clearly demonstrated the advantages of performing Brillouin spectroscopy in the transparent regime. However, the Brillouin spectrometer used in those experiments was not well adapted for more elaborate experiments. This encouraged us to optimize our Brillouin spectrometer to take full advantage of near infrared Brillouin scattering. The details of the modifications and the optimization of the tandem triple-pass Fabry-Perot interferometer can be found elsewhere.[25] The schematic experimental setup for the Brillouin experiments is shown in Fig. 2.

With the use of the improved spectrometer and the photon counting detector (Si avalanche photodiode with a quantum efficiency of 30% in the NIR), we reduce the acquisition times considerably. Measuring in the transparent region enables us to use all the scattering geometries usually employed for Brillouin spectroscopic studies. Figure 3 shows the scattering geometries used in the experiments and the corresponding combination of elastic moduli. In Ref. 13 only backscattering and near backscattering geometries have been used and hence the detected quasitransverse acoustic phonons are weak in intensity.

It is well known from the literature,[26,27] that for rather small scattering angles ($\theta \leqslant 90°$) the effect of a finite collec-

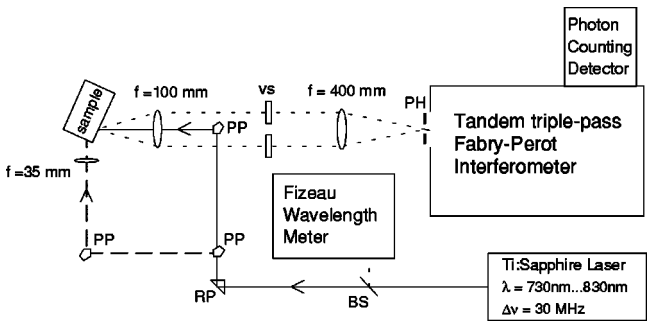

FIG. 2. Near infrared Brillouin scattering setup. BS: beam splitter. RP: right-angle prism. PP: penta prism. *f*: focal length of lenses. PH: pinhole (250 μm). The vertical slit (vs) aperture is used in the right-angle geometry to avoid aperture broadening and shifts.

tion aperture causes a broadening and a systematic shift of the Brillouin lines to lower frequencies. For this reason we insert a vertical slit after the collection lens (Fig. 2), to obtain a rather small collection aperture[28] of $2\Delta\theta \leqslant 0.6°$ (inside the sample) for the right-angle geometry.[29]

The exact Brillouin shifts are determined by fitting Lorentzian curves to the peaks and by averaging the positions on the stokes and antistokes side in the spectra. To minimize random errors, we recorded Brillouin spectra at several excitation wavelengths between 730 nm and 830 nm. The calculated elastic constants are averaged over this wavelength range. Typical standard deviations of the mean values

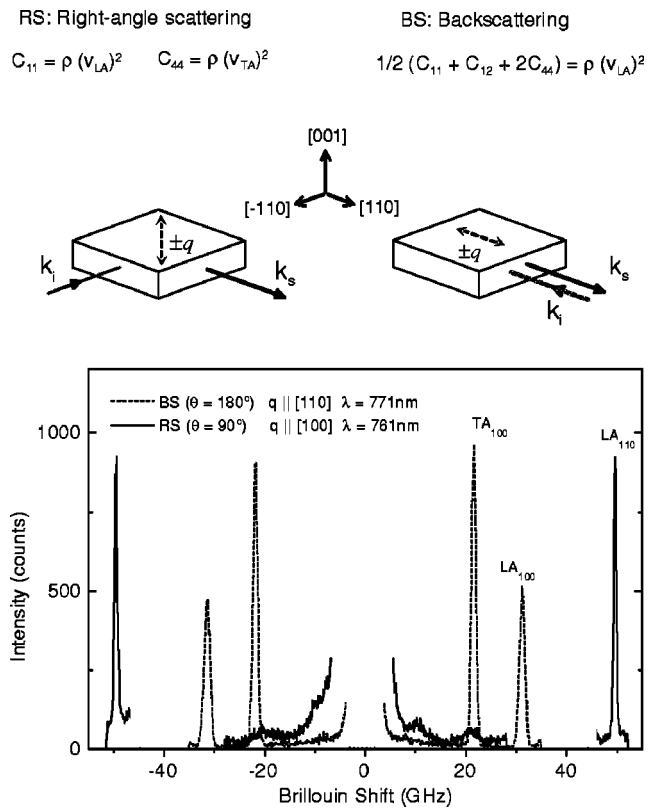

FIG. 3. Scattering geometries and room temperature Brillouin spectra of AlAs. The LA and TA phonons propagating along the [100] crystal direction are observed in the right-angle scattering geometry (RS) and the LA phonon propagating along the [110] direction is observed in the backscattering geometry (BS).

are 0.25%. The measurements are performed at a temperature of (22.5 ± 0.5) °C with excitation powers below 50 mW. The sound velocities v are calculated from the measured Brillouin shift $\Delta\nu$, according to

$$v = \frac{\lambda}{2n(\lambda)\sin(\theta/2)}\Delta\nu, \tag{1}$$

where the scattering angle is θ, the excitation wavelength is λ, and the refractive index is $n(\lambda)$. The elastic constants are calculated from the expressions shown in Fig. 3 for the corresponding scattering geometry.

The crystal density $\rho(x)$ is derived from the measured lattice constants of the strained tetragonal unit cell and the molecular weight of $Al_xGa_{1-x}As$. The refractive index dispersion $n(\lambda)$ is determined by a grating coupling technique, which measures the effective index of leaky modes propagating in the improper waveguide structure formed by the $Al_xGa_{1-x}As$ layer on top of the GaAs substrate.[30] Since the used scattering geometries are taking advantage of this waveguide effect, this technique is very well adapted for our problem, because it allows us to determine directly the effective index of the sample with an accuracy of $\Delta n = 0.0005$. The excitation wavelength is measured with a Fizeau wavelength meter with an absolute accuracy of 0.01 nm. To minimize the error in the scattering angle for the right-angle geometry, we use penta prisms for the beam deflection, shown in Fig. 2. This guarantees that the scattering angle is exactly $90° \pm 0.15°$. Figure 3 shows two typical Brillouin spectra of AlAs in backscattering and right-angle geometry. The signal to noise ratio is much lower for the backscattering spectrum, because of a much higher Rayleigh-scattering background (which has been subtracted here for comparison) resulting from surface imperfections. Particularly for AlAs, after measurement times >4 h the cleaved surface is damaged so heavily by oxidation that it is nearly impossible to detect peaks from bulk phonons. Instead additional broad peaks around 10 and 20 GHz appeared. These peaks could possibly result from oxide layers at the cleaved AlAs surface.

III. RESULTS

A. Elastic constants

The results of the Brillouin measurements are summarized in Fig. 4. For the longitudinal acoustic sound velocities in [010] and [110] directions, we observe nearly no change from GaAs to AlAs [Fig. 4(a)]. Accordingly, we propose a composition independent value of 118.9 ± 0.7 GPa for C_{11}. For the shear elastic constants we observe a nonlinear increase of C_{12} and a nearly linear decrease of C_{44} from GaAs to AlAs. The elastic constant dependence on Al composition (as determined by ICP-AES) is fitted by polynomials to our data:

$$C_{11}(x) = (118.9 \pm 0.7) \quad \text{GPa},$$

$$C_{12}(x) = (53.7 + 4.85x + 11.9x^2 - 13.0x^3) \quad \text{GPa}, \tag{2}$$

$$C_{44}(x) = (59.1 - 1.88x) \quad \text{GPa}.$$

The Poisson ratio for a tetragonal distortion of a cubic layer grown on a (001) substrate is defined as[31]

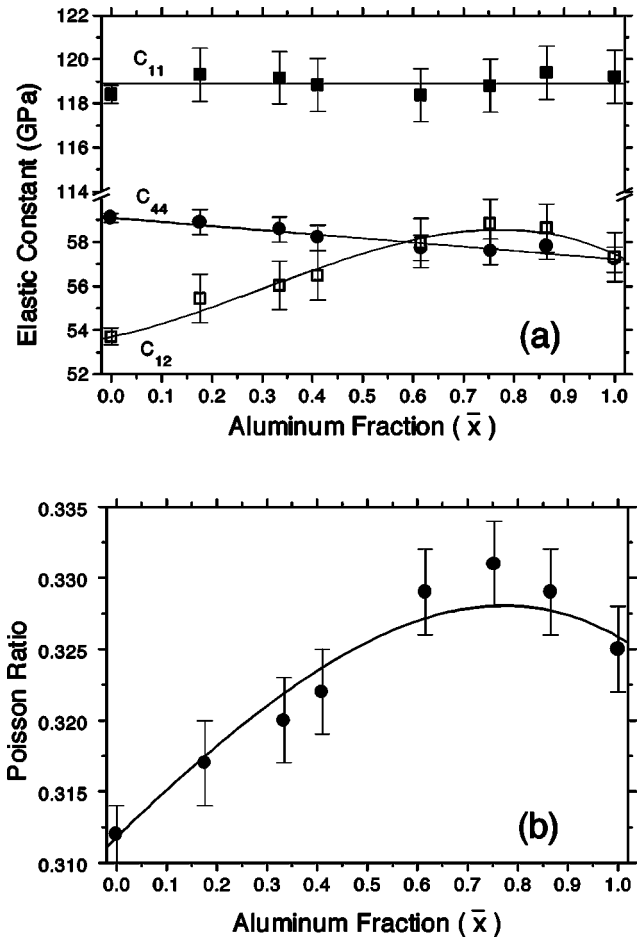

FIG. 4. Elastic constants (a) and Poisson ratio (b) of $Al_xGa_{1-x}As$ as a function of composition ($\bar{x}$). The full lines give the result of the polynomial fits according to Eq. (2).

$$\nu(x)=\frac{C_{12}(x)}{C_{12}(x)+C_{11}(x)}. \tag{3}$$

Figure 4(b) shows the compositional dependence of $\nu(x)$. For AlAs we get $\nu=0.325\pm0.004$, in good agreement with our previous study[13] and with values obtained by HRXRD on AlAs layers with different degrees of relaxation[32,10] or grown on differently oriented substrates.[33] As shown in Fig. 4b, $\nu(x)$ could be considered to vary linearly with composition for $x<0.8$, but for $x=1$ a clear decrease is observed.

Table II shows the complete set of elastic constants for all samples investigated. The quoted errors are calculated from the relative errors for the Brillouin shift ($\delta\Delta\nu/\Delta\nu=3.0\times10^{-3}$), the scattering angle ($\delta\theta/\theta=5.5\times10^{-4}$), the refractive index ($\delta n/n=1.3\times10^{-4}$) and the wavelength ($\delta\lambda/\lambda=1.3\times10^{-5}$). Some of the values on the elastic parameters listed in Table II are not consistent with our previous study.[13] The reason for these discrepancies is mainly due to systematic errors in the refractive index and due to the phonon angular dispersion,[25] which has not been considered in Ref. 13. In an earlier investigation,[12] values for C_{11} have been found which are up to 3% lower than in the present study. Subsequent x-ray characterization of the samples used there has revealed a poor structural quality. For this reasons we believe that the results on C_{11} presented there suffer from systematic errors in the refractive index and the crystal density caused by composition inhomogeneities and misfit dislocations.

From elasticity theory it is well known that statically stressed crystals show deviations in their sound velocities with respect to their unstrained state.[36] The parameters describing this effect are the third order elastic constants. To estimate the change in effective elastic constants of a biaxially stressed $Al_xGa_{1-x}As$ layer, we use the differential equations for particle motion in stressed cubic crystals.[37] Since the third order elastic constants of $Al_xGa_{1-x}As$ and AlAs are not known, we use the values of GaAs[39] for numerical calculations.

Figure 5 shows the expected relative change of the second order elastic constants C_{11}, C_{12}, and C_{44} as a function of biaxial stress σ. As it is for hydrostatic pressure,[40] the effective elastic constants ϱv^2 of the biaxially stressed crystal increase with respect to the unstressed state. However the change is rather small for typical values of $\sigma<0.174$ GPa that corresponds to a fully stressed AlAs layer on GaAs. Nevertheless we could verify the expected effect by Brillouin measurements on a completely relaxed and free standing $Al_{0.75}Ga_{0.25}As$ film (sample *N*). For these measurements the substrate is removed from the layer by chemical etching and

TABLE II. Elastic constants and relaxed lattice parameters of $Al_xGa_{1-x}As$. The values for the Al mole fraction $\bar{x}$ are taken from the ICP-AES analysis where available. For samples P and F the compositions determined by PL are used. The elastic constants of GaAs are taken from Cottam *et al.* (Ref. 34).

Sample	Al content ($\bar{x}$)	C_{11} (GPa)	C_{12} (GPa)	C_{44} (GPa)	Poisson ratio ν	Lattice parameter (pm)
J	GaAs	(118.4±0.4)	(53.7±1.5)	(59.1±0.2)	(0.312)	565.359±0.004
P	0.095±0.005	(118.9±0.8)	(54.6±1.8)	(59.0±0.5)	(0.315±0.005)	565.450±0.007
B	0.176±0.005	119.3±0.7	55.4±1.0	58.9±0.4	0.317±0.004	565.516±0.006
F	0.225±0.005	119.1±0.7	55.4±1.0	58.4±0.4	0.317±0.004	565.560±0.006
C	0.334±0.005	119.2±0.7	56.0±1.0	58.6±0.4	0.320±0.004	565.658±0.006
A	0.410±0.005	118.8±0.7	56.5±1.0	58.2±0.4	0.322±0.004	565.714±0.007
D	0.615±0.005	118.4±0.7	58.0±1.0	57.7±0.4	0.329±0.004	565.884±0.007
N	0.753±0.005	118.8±0.7	58.8±1.0	57.6±0.4	0.331±0.004	565.991±0.008
Q	0.865±0.005	119.4±0.7	58.6±1.0	57.8±0.4	0.329±0.004	566.065±0.011
E	AlAs	119.3±0.7	57.2±1.0	57.2±0.4	0.324±0.004	566.171±0.009

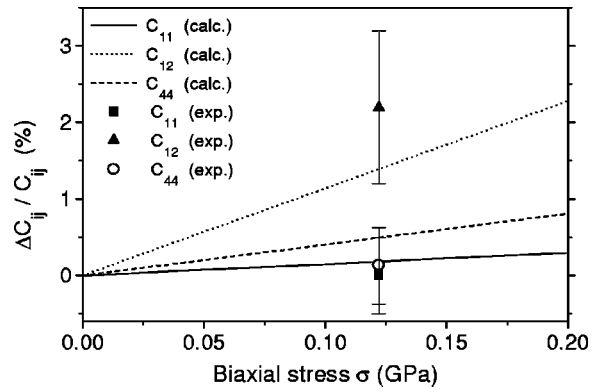

FIG. 5. Measured and estimated relative change in elastic constants due to biaxial stress σ. The experimental uncertainty in the elastic constants of the $Al_{0.75}Ga_{0.25}As$ sample is approximately $\pm 1\%$ for the change in C_{12}, and $\pm 0.5\%$ for the change in C_{11} and C_{44}.

a small specimen (<1 mm^2) of the thin film is pinned with adhesive on the sample holder. To ensure that the film is freely standing in an unstressed state, it is fixed on a single point only. All three elastic constants of the relaxed film are obtained by employing the scattering geometries shown in Fig. 3. The elastic constants thus obtained are compared to the stressed layer. The results are given in Fig. 5. The amount of biaxial stress ($\sigma = 0.122$ GPa) is calculated from the strain field, determined by HRXRD, and the elastic constants. Considering the measurement uncertainties and the poorly known third order elastic constants, the agreement between theory and experiment is reasonable. The use of the GaAs third order elastic constants is thus justified for the complete composition range. Since the change of the effective elastic constants due to stress is only slightly larger than the absolute measurement uncertainties, we neglect it altogether and use the clamped elastic parameters obtained on the strained layers. It should be noted that the small strain effect cannot be responsible for the experimentally observed downward bowing of C_{12} and the Poisson ratio observed for $x > 0.8$.

B. Lattice parameter

The complete metric of the tetragonally strained epitaxial layers and the substrate is measured by HRXRD, as described in Sec. II B. All epitaxial layers are almost fully strained showing no deviation from tetragonality, as judged from reflections belonging to zones perpendicular to each other. The degree of relaxation[38] is lower than 10% for all samples except for the 10 μm thick sample C, where we noted 15% relaxation. From the measured Bragg angles Θ_{00l} of the symmetric reflections $00l$ we obtain the tetragonal lattice parameter perpendicular to the layer plane

$$c = \frac{\Lambda l}{2 \sin \Theta_{00l}}, \tag{4}$$

and from the asymmetric reflections hkl the ratio c/a of the lattice constants perpendicular and parallel to the layer plane is obtained from

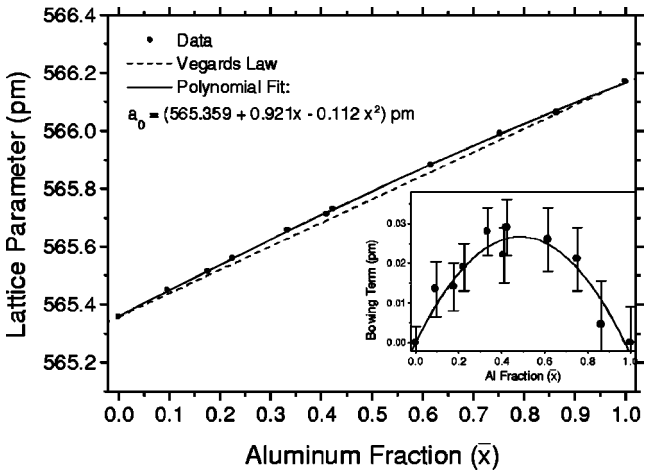

FIG. 6. Relaxed lattice parameter of $Al_xGa_{1-x}As$ as a function of composition ($\bar{x}$). The inset shows the quadratic bowing.

$$c/a = \left[\left(\frac{1}{\cos^2 \phi_{hkl}} - 1 \right) \frac{l^2}{h^2 + k^2} \right]^{1/2}, \tag{5}$$

where ϕ_{hkl} is the angle between the hkl plane and the (001) growth surface. The relaxed lattice parameter a_0 is obtained by mathematical relaxation of the tetragonal distortion using the relation

$$a_0 = c \left(\frac{1 + Ka/c}{1 + K} \right), \tag{6}$$

where

$$K = 2 \frac{\nu}{1 - \nu} = 2 \frac{C_{12}}{C_{11}} \tag{7}$$

is the elastic correction factor. It is calculated from the experimentally determined values of the Poisson ratio ν (Table II) for each sample separately. Figure 6 shows the relaxed lattice parameter plotted versus the Al compositions $\bar{x}$. The deviation from the linear dependence (dotted line) is distinct. An analytical relation for the compositional dependence of the relaxed $Al_xGa_{1-x}As$ lattice parameter is given by a quadratic fit:

$$a^0_{Al_xGa_{1-x}As}(x) = 565.359 + 0.921(x - 0.122x^2) \quad \text{pm}. \tag{8}$$

The inset of Fig. 6 shows the difference between the quadratic fitting function and the linear relation of Vegard's law. It clearly shows symmetric bowing in $a_0(x)$. At $x = 0.5$ the relative bowing $\Delta a_0(x)/a_0(x)$ has a maximum of approximately 4.6×10^{-5}, a value which is easily resolved by our accurate HRXRD measurements, having uncertainties for the relaxed lattice parameters of <15 ppm. The bowing term measured in this work is slightly smaller than that proposed by Wasilewski *et al.*[11] The reason is because they assumed a linear variation of the Poisson ratio and bowing has been completely attributed to $a_0(x)$. Our Brillouin measurements reveal an upward bowing in the Poisson ratio, resulting in a reduced bowing of $a_0(x)$.

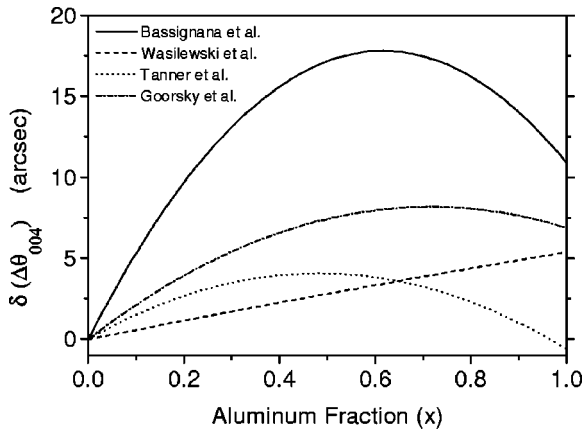

FIG. 7. Deviations between the $\Delta\theta_{004}(x)$ relation from this work [Eq. (9)] and some of the recently published relations.

IV. DISCUSSION

A. Composition measurements by HRXRD

To demonstrate the consequences of the quadratic bowing in $a_0(x)$ for routine composition measurements by HRXRD, we determine the composition value (x_{XRD}) from the relaxed lattice parameters under the assumption of Vegard's law. These values are listed in Table II for each sample. A comparison between x_{XRD} and the composition obtained by ICP-AES or PL and Raman spectroscopy shows that the HRXRD compositions based on Vegard's law are approximately 3.2 at. % higher at the 50% Al level. This difference is considerably larger than the typically quoted 1% uncertainty for the Al composition determination by HRXRD.[1]

For routine compositional measurements, usually the angular separation between the substrate and the layer is measured by 004 reflection rocking curves. To give a functional equation for the 004 reflection peak separation we extract from our data the following relation for a completely strained $Al_xGa_{1-x}As$ layer on an unstrained (001) GaAs substrate:

$$\Delta\theta_{004}(x) = 425.9x - 47x^2 \qquad \text{arcsec.} \tag{9}$$

For a completely strained AlAs layer we obtain a peak separation of $\Delta\theta_{004} = 377.9 \pm 2.6$ arcsec, in agreement with that determined by Tanner *et al.*[5] The corresponding relaxed lattice mismatch between GaAs and AlAs is determined to be

$$m_0 = \frac{a_0(\mathrm{AlAs}) - a_0(\mathrm{GaAs})}{a_0(\mathrm{GaAs})} = (14.36 \pm 0.10) \times 10^{-4}, \tag{10}$$

in reasonable agreement with Refs. 10, 32, and 33. The directly measured lattice parameter of the semi-insulating GaAs substrates of $a_0(\mathrm{GaAs}) = (565.359 \pm 0.004)$ pm (at 22.5 °C) is in perfect agreement with the recommended value for stoichiometric, undoped GaAs quoted in the latest data review.[41]

With the exact knowledge on the compositional dependence of the relaxed lattice parameter and the Poisson ratio we now can explain some of the discrepancies in the literature. Since crystal growers have for almost a decade used the 004 reflection peak separation to monitor the Al-composition, we show in Fig. 7 the differences between Eq. (9) and some of the recently published relations of $\Delta\theta_{004}(x)$. Compared to the results of Tanner *et al.*[5] and Goorsky *et al.*,[6] who used a two-parameter fit to the quadratic dependence of $\Delta\theta_{004}(x)$, we get a maximum deviation of 4.1 arcsec and 8.2 arcsec, respectively. The agreement with Tanner *et al.*[5] is reasonable within experimental uncertainties. The rather large discrepancies with Goorsky *et al.*[6] may be attributed to systematical errors in their composition determination by PL and electron microprobe. Since in both studies the 004 peak separation and the layer composition has been determined independently, the proposed $\Delta\theta_{004}(x)$ relations work quite satisfactorily for routine compositional measurements on fully strained layers, irrespective of the validity of Vegard's law. But Tanner *et al.*[5] and Goorsky *et al.*[6] also used their $\Delta\theta_{004}(x)$ dependence to determine the AlAs Poisson ratio under the assumption of a linear composition dependence of the relaxed lattice parameter and the Poisson ratio. Since these assumptions are not valid, they obtained erroneous results of $\nu_{AlAs} = 0.28$ (Ref. 5) and $\nu_{AlAs} = 0.275$ (Ref. 6). Because of the incorrect Poisson ratio, the AlAs relaxed lattice parameters quoted there are also incorrect.

The difference between our result and the functional equation obtained by Wasilewski *et al.*[11] increases linearly with composition, reaching a maximum deviation of 5.4 arcsec for AlAs. Since our compositional measurements by PL and Raman spectroscopy are based on the calibration curves of Wasilewski *et al.*, we already confirmed the good agreement of their composition calibration with our ICP-AES results. Hence we attribute any difference to the HRXRD measurements. Although the differences are rather small, we assume the linear increase might be attributed to partial relaxation of the layers with high Al contents and to substrate deformation, which were neglected in most of the studies published up to now and in particular in Ref. 11, where only symmetric 004 reflections have been used. We feel that studies claiming high accuracy in metric/composition determination should be looked upon with suspicion when only symmetric 00*l* peaks or peak splittings (layer/substrate) were used to obtain the strain field of the layer. For example, neglecting the strain in a 635 μm (001) GaAs wafer covered with a 1 μm elastically strained AlAs layer results in a peak separation which would be 2.6 arcsec too low.

Comparing our results to the measurements by Bassignana *et al.*[1] we get unacceptable large differences of up to 18 arcsec. Bassignana *et al.* measured a linear relationship for $\Delta\theta_{004}(x)$, which would mean that Vegards law is strictly fulfilled and the Poisson ratio of $Al_xGa_{1-x}As$ has the same value as GaAs for the complete composition range. Both findings are in clear conflict with our results. Since the observed difference $\delta(\Delta\theta_{004})(x)$ has a linear and a quadratic part, we attribute it to the partial relaxation of their layers and systematic errors in the composition determination by electron probe microanalysis, respectively. From Fig. 2 in Ref. 1 it is obvious that substantial relaxation is present in their layers, since for AlAs peak separations as low as ≈ 330 arcsec have been measured.

B. Force constants and ionicity of AlAs

Simple trends in the elastic properties of zinc-blende semiconductors have been investigated by Keyes[42] and

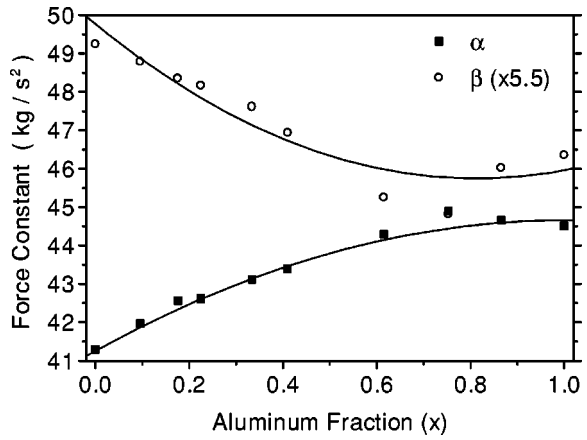

FIG. 8. Effective bond-bending (β, multiplied by 5.5) and bond-stretching (α) force constants as a function of composition (x). The solid lines are second order polynom fits and serve to illustrate the small bowing in $\alpha(x)$ and $\beta(x)$.

Martin.[43] In a simplified valence-force-field (VFF) model[44] the elastic constants of binary zinc-blende semiconductors can be expressed in terms of bond-stretching (α) and bond-bending (β) forces and a Coulomb contribution term.[43] Using Eq. (11) of Ref. 43 and the measured elastic constants and lattice parameter we calculate the effective medium force constants α and β shown in Fig. 8. To calculate the Coulomb force contributions for GaAs and AlAs we use the LO and TO phonon frequencies from Ref. 11, and for intermediate compositions we interpolate linearly.

For the effective bond-bending force constant we observe a decrease with increasing Al content, implying that the directional character of the Al-As bonds is reduced compared to the Ga-As bonds. A small bowing is observed for both, bond-stretching and bond-bending forces as a function of composition. As was shown[42,43] the reduced elastic constants of zincblende semiconductors follow simple trends, and in particular the ratio of β/α is a linear function of the bond ionicity, f_i. For β/α we observe a decrease of 14.5% from GaAs to AlAs. Thus with[43] $\beta/\alpha \propto (1-f_i)$ the ionicity of AlAs is increased by the same amount. Using the ionicity of GaAs from Philips[45] [$f_i(\mathrm{GaAs})=0.310$] we obtain $f_i(\mathrm{AlAs})=0.355$.

For the bulk modulus in III-V zinc-blende semiconductors an empirical formula was suggested by Cohen:[46]

$$B=\tfrac{1}{3}(C_{11}+2C_{12})=1949/d^{3.5}, \qquad (11)$$

where the nearest neighbor distance d is in Å and B is in GPa. From our elastic constants, we obtain bulk moduli which increase nonlinearly with the Al content. The bulk modulus of AlAs is approximately 3.5% higher than that of GaAs, totally in contradiction to the $d^{-3.5}$ scaling of Eq. (11). In Cohen's formula the effect of ionicity is not included explicitly, so we attribute the increase in B from GaAs to AlAs to the increase in ionicity.

C. Violation of Vegard's law

As pointed out in Refs. 47 and 48 deviations from Vegard's law are expected in systems with length mismatch and different force constants for the binary constituents, as we observed it experimentally in the GaAs-AlAs system (Fig. 8). Deviations from Vegard's law have been found experimentally[11,49–51] and theoretically[52–56] in various semiconductor compounds, such as $Si_{1-x}Ge_x$, $Si_{1-x-y}Ge_xC_y$ and $GaAs_xSb_{1-x}$. For the $Al_xGa_{1-x}As$ system, a relatively small bowing in $a_0(x)$ is expected. For example, the simple formula [Eq. (36) of Ref. 56] for the effective bond length obtained by Chen *et al.*, based on the internal strain energy of atomic clusters, predicts a relative quadratic bowing of $\Delta a_0(0.5)/a_0(0.5)\approx 4\times 10^{-6}$. However, the observed bowing in the $Al_xGa_{1-x}As$ lattice parameter is an order of magnitude larger, indicating that the simple cluster model is not appropriate for quantitative predictions. Correspondingly, the simple formulas obtained from elasticity theory, summarized in Ref. 49, predict the correct sign of the bowing, but produce values which are typically an order of magitude too low.

Qualitative explanations for the violation of Vegard's law have been given by Fong *et al.*[35] on the basis of bond-bending and bond-stretching forces. They found that the difference in the bond-bending forces is the critical quantity separating a quadratic bowing in $a_0(x)$ from an *S*-shaped one. They showed that all materials with $\beta_r=(\beta_1-\beta_0)/(\beta_1+\beta_0)>-0.071$ should exhibit a *S*-shape (cubic) bowing, as observed in the $InAs_xSb_{1-x}$ system[57] (β_0 and β_1 are the bond-bending forces of the binary compounds, InAs and InSb, respectively). For the AlAs-GaAs system we calculate $\beta_r=-0.02$, and hence a *S*-shape bowing would be expected. But our experiments clearly show a quadratical convex bowing. Possible reasons for the failure of the simple model of Fong *et al.* to predict deviations from Vegard's law have already been pointed out in Ref. 59.

In Ref. 60 a VFF model is used to derive analytical expressions for the mean average lengths parameters in ternary compounds. Bowing in the compositional dependence is predicted for systems with unequal force constants for the binary constituents, and the magnitude of the bowing parameter is proportional to the force constant difference and the length mismatch. With the force constant parameters of GaAs and AlAs we obtain for $Al_xGa_{1-x}As$ a maximum bowing in the lattice parameter at $x=0.5$ of $\Delta a_0(0.5)=0.45\times 10^{-4}$ Å. This value should be compared to our experimentally observed bowing of 2.6×10^{-4} Å. Obviously the model of Cai and Thorpe[60] predicts a bowing with the correct sign, but still a factor of 5 too small. This discrepancy may be attributed to anharmonic effects, but in particular for the GaAs-AlAs system the lattice mismatch is very small, thus the harmonic approximation used in the VFF models should hold.

To conclude, none of the various models predicts the magnitude of the experimentally observed bowing in the lattice parameter of $Al_xGa_{1-x}As$ correctly. Since all the models based on elasticity theory neglect the charge transfer,[58,48] an effect playing an important role for the bowing in $Si_{1-x-y}Ge_xC_y$,[55] and in metallic alloys,[48] we surmise that charge transfer dominates the contribution leading to deviatons from Vegard's law in the AlAs-GaAs system. This could be verified by computer simulations such as the embedded-atom method which has been employed to explain the violation of Vegard's law in metallic alloys.[48]

It is interesting to note here that the relative bowing in $a_0(x)$ at $x=0.5$, defined as

$$b=\frac{a_0(0.5)-1/2[a_0(1)+a_0(0)]}{a_0(1)-a_0(0)}, \tag{12}$$

has nearly the same amount (but opposite sign) for $Al_xGa_{1-x}As(b=0.032\pm0.009)$ and $Si_{1-x}Ge_x$ ($b=-0.030$, Ref. 50).

V. SUMMARY

The present study investigates the elastical and structural parameters of $Al_xGa_{1-x}As$ epitaxial layers by combining the results of near infrared Brillouin scattering, HRXRD and compositional analysis. The relaxed lattice parameters of $Al_xGa_{1-x}As$ are precisely determined from the measured elastic constants and strained lattice parameters. The independent determination of the Al content demonstrates the deviation from Vegard's law, and permits a direct determination of the quadratic bowing term for the relaxed lattice parameter. The consequences of the small bowing for routine composition determination by HRXRD are discussed in detail and some of the discrepancies present in the literature are reconciled. A comparison of the experimentally observed bowing with some simple models on the departure from Vegard's law shows that none of them predicts the correct order of magnitude.

ACKNOWLEDGMENTS

We wish to acknowledge H. Siegwart (PSI) for technical assistance with the Brillouin spectrometer, H. Auderset (PSI) for his help with the Raman measurements, and A. Vonlanthen (PSI, CSEM Zürich) for the expert sample preparation. S. Bürkner and K. Winkler (both from the FHG-IAF) are acknowledged for the MOCVD sample growth. We thank Bruce Patterson (PSI) and Patricia Schroeter (University of Zürich, PSI) for interesting discussions and for their suggestion to use the ICP-AES for compositional analysis.

[1] For a recent review, see, e.g., I.C. Bassignana, D.A. Macquistain, R.W. Streater, G.C. Hillier, R. Packwood, and V. Moore, J. Cryst. Growth **172**, 25 (1997).
[2] W.J. Bartels and W. Nijman, J. Cryst. Growth **44**, 518 (1978).
[3] A. Leiberich and J. Levkoff, J. Cryst. Growth **100**, 330 (1990).
[4] K.H. Chang, C.P. Lee, J.S. Wu, D.G. Liu, D.C. Liou, M.H. Wang, L.J. Chen, and Mario A. Marais, J. Appl. Phys. **70**, 4877 (1991).
[5] B.K. Tanner, A.G. Turnbull, C.R. Stanley, A.H. Kean, and M. McElhinney, Appl. Phys. Lett. **59**, 2272 (1991).
[6] S.M. Goorsky, T.F. Kuech, M.A. Tischler, and R.M. Potemski, Appl. Phys. Lett. **59**, 2269 (1991).
[7] M.D. Lind, C.W. Farley, G.J. Sullivan, and R.W. Grant, J. Appl. Phys. **74**, 5910 (1993).
[8] G.S. Solomon, D. Kirillov, H.C. Chui, and J.S. Harris, Jr., J. Vac. Sci. Technol. B **12**, 1078 (1994).
[9] L. Vegard, Z. Phys. **5**, 17 (1921).
[10] R.P. Leavitt and F.J. Towner, Phys. Rev. B **48**, 9154 (1993).
[11] Z.R. Wasilewski, M.M. Dion, D.J. Lockwood, P. Pole, R.W. Streater, and A.J. SpringThorpe, J. Appl. Phys. **81**, 1683 (1997).
[12] M. Krieger, H. Sigg, and F.K. Reinhart, Solid State Commun. **88**, 267 (1993).
[13] M. Krieger, H. Sigg, N. Herres, K. Bachem, and K. Köhler, Appl. Phys. Lett. **66**, 682 (1995).
[14] B. Starbuck, E. Cathers, M.W. Routh, and M.W. Tikkanen, Semicond. Int. **1987**, 209.
[15] The ICP-AES is available as a service from *Alusuisse Technology*, CH-8212 Neuhausen a. Rheinfall, Switzerland: Contact: E. Sutter.
[16] G.C. DeSalvo, W.F. Tseng, and J. Comas, J. Electrochem. Soc. **139**, 831 (1992).
[17] R.A. Logan and F.K. Reinhart, J. Appl. Phys. **44**, 4172 (1973).
[18] J.J. LePore, J. Appl. Phys. **51**, 6441 (1980).
[19] W. Bartels, J. Vac. Sci. Technol. B **1**, 338 (1983).
[20] W.L. Bond, Acta Crystallogr. **13**, 814 (1960).
[21] S. Grosswig, K.-H. Jäckel, R. Kittner, B. Dietrich, and U. Schellenberger, Crystal Res. & Technol. **20**, 1093 (1985); S. Grosswig, J. Härtwig, U. Alter, and A. Christoph, *ibid.* **18**, 501 (1983).
[22] N. Herres, A. Dommann, M. Krieger, H. Sigg, K. Bachem, and K. Köhler (unpublished).
[23] M. Krieger, H. Sigg, F. Morier-Genoud, D. Martin, and F.K. Reinhart, in *Proceedings of the 22nd International Conference on the Physics of Semiconductors, Vancouver, 1994*, edited by D. Lockwood (World Scientific, Singapore, 1995), Vol. 2, pp. 959–962.
[24] J.R. Sandercock, in *Light Scattering in Solids III*, edited by M. Cardona and G. Güntherodt, Vol. 51 of Springer Topics in Applied Physics (Springer, Berlin, 1982), pp. 173–206.
[25] S. Gehrsitz, H. Sigg, H. Siegwart, M. Krieger, C. Heine, R. Morf, F.K. Reinhart, W. Martin, and H. Rudigier, Appl. Opt. **36**, 5355 (1997).
[26] W.F. Oliver, C.A. Herbst, S.M. Lindsay, and G.H. Wolf, Rev. Sci. Instrum. **63**, 1884 (1991).
[27] H.G. Danielmayer, J. Acoust. Soc. Am. **47**, 151 (1970).
[28] Using the full lens aperture, corresponding to an internal collection aperture of $2\Delta\theta=6°$, instead of the vertical slit aperture resulted in a $\approx$0.4% shift of the Brillouin lines to lower frequencies.
[29] Christian Gigault, private communication (see http://www.uoguelph.ca/~cgigault/aper/index.html)
[30] S. Gehrsitz, H. Sigg, A. Vonlanthen, N. Herres, C. Gourgon, and F. K. Reinhart (unpublished).
[31] W.A. Brantley, J. Appl. Phys. **44**, 534 (1973).
[32] C. Bocchi, C. Ferrari, P. Franzosi, A. Bosacchi, and S. Franchi, J. Cryst. Growth **132**, 427 (1993).
[33] L. De Caro, C. Giannini, L. Tapfer, H.-P. Schönherr, L. Däweritz, and K.-H. Ploog, Solid State Commun. **108**, 77 (1998).
[34] R.I. Cottam and G.A. Saunders, J. Phys. C **6**, 2105 (1973).
[35] C.Y. Fong, W. Weber, and J.C. Phillips, Phys. Rev. B **14**, 5387 (1976).
[36] R.N. Thurston and K. Brugger, Phys. Rev. **133**, A1604 (1964).
[37] T. Bateman, W.P. Mason, and H.J. McSkimin, J. Appl. Phys. **32**, 928 (1961).
[38] M.A.G. Halliwell, M.H. Lyons, S.T. Davey, M. Hockly, C.G.

Tuppen, and C.J. Gibbings, Semicond. Sci. Technol. **4**, 10 (1989).
[39] D. J. Dunstan, in *Properties of Gallium Arsenide*, EMIS Datareviews Series No. 16, 3rd ed., edited by M. R. Brozel and G. E. Stillman (INSPEC, London, 1996), pp. 16–20.
[40] R.Ramji Rao and A. Padmaja J. Appl. Phys. **62**, 440 (1987).
[41] *Properties of Gallium Arsenide* (Ref. 39), p. 9.
[42] R.W. Keyes, J. Appl. Phys. **33**, 3371 (1962).
[43] R.M. Martin, Phys. Rev. B **1**, 4005 (1970).
[44] M.J.P. Musgrave and J.A. Pole, Proc. R. Soc. London, Ser. A **268**, 474 (1962).
[45] J.C. Phillips, Phys. Rev. Lett. **20**, 550 (1968); J. C. Phillips, *Bonds and Bands in Semiconductors* (Academic Press, New York, 1973).
[46] M.L. Cohen, Phys. Rev. B **32**, 7988 (1985).
[47] M.F. Thorpe and E.J. Garboczi, Phys. Rev. B **42**, 8405 (1990).
[48] N. Mousseau and M.F. Thorpe, Phys. Rev. B **45**, 2015 (1992).
[49] J.P. Dismukes, L. Ekstrom, and R.J. Paff, J. Phys. C **68**, 3021 (1964).
[50] E. Kasper, A. Schuh, G. Bauer, B. Holländer, and H. Kibbel, J. Cryst. Growth **157**, 68 (1995).
[51] M. Berti, D. De Salvador, A.V. Drigo, F. Romanato, J. Stangl, S. Zerlauth, F. Schäffler, and G. Bauer, Appl. Phys. Lett. **72**, 1602 (1998).
[52] G. Theodorou, P.C. Kelires, and C. Tserbak, Phys. Rev. B **50**, 18 355 (1994).
[53] P.C. Kelires, Phys. Rev. B **55**, 8784 (1997).
[54] L.G. Ferreira, Su-Huai Wei, and A. Zunger, Phys. Rev. B **40**, 3197 (1989).
[55] J.L. Martins and A. Zunger, Phys. Rev. Lett. **56**, 1400 (1986).
[56] A.-B. Chen, A. Sher, and M.A. Berding, Phys. Rev. B **37**, 6285 (1988).
[57] J.C. Wooley and J. Warner, J. Electrochem. Soc. **111**, 1142 (1942).
[58] K.A. Gscheidner, Jr. and G.H. Vineyard, J. Appl. Phys. **33**, 3444 (1962).
[59] J.C. Mikkelsen, Jr. and J.B. Boyce, Phys. Rev. B **28**, 7130 (1983).
[60] Y. Cai and M.F. Thorpe, Phys. Rev. B **46**, 15 879 (1992).